Metabolism Clinical and Experimental 117 (2021) 154707

Contents lists available at ScienceDirect

Metabolism Clinical and Experimental

journal homepage: www.metabolismjournal.com

Basic Science

# Elafibranor improves diet-induced nonalcoholic steatohepatitis associated with heart failure with preserved ejection fraction in Golden Syrian hamsters

François Briand [a,*], Julie Maupoint [b], Emmanuel Brousseau [a], Natalia Breyner [a], Mélanie Bouchet [a], Clément Costard [b], Thierry Leste-Lasserre [c], Mathieu Petitjean [d], Li Chen [d], Audrey Chabrat [e], Virgile Richard [e], Rémy Burcelin [f], Caroline Dubroca [b], Thierry Sulpice [a,b]

[a] Physiogenex, 280 rue de l'Hers, ZAC de la Masquère, 31750 Escalquens, France
[b] Cardiomedex, 280 rue de l'Hers, ZAC de la Masquère, 31750 Escalquens, France
[c] Neurocentre Magendie, 146 rue Léo Saignat, 33077 Bordeaux cedex, France
[d] PharmaNest, 100 Overlook Center, FL2, Princeton, NJ 08540, United States of America
[e] Sciempath Labo, 7 rue de la Gratiole, 37270 Larcay, France
[f] Inserm U1048 CHU Rangueil, BP 84225, 31432 Toulouse Cedex 4, France

ARTICLE INFO

*Article history:*
Received 16 October 2020
Accepted 7 January 2021

*Keywords:*
Nonalcoholic steatohepatitis
Fibrosis
Heart failure
Diastolic dysfunction
Hamster

ABSTRACT

*Background:* Cardiovascular disease is the leading cause of deaths in nonalcoholic steatohepatitis (NASH) patients. Mouse models, while widely used for drug development, do not fully replicate human NASH nor integrate the associated cardiac dysfunction, i.e. heart failure with preserved ejection fraction (HFpEF). To overcome these limitations, we established a nutritional hamster model developing both NASH and HFpEF. We then evaluated the effects of the dual peroxisome proliferator activated receptor alpha/delta agonist elafibranor developed for the treatment of NASH patients.

*Methods:* Male Golden Syrian hamsters were fed for 10 to 20 weeks with a free choice diet, which presents hamsters with a choice between control chow diet with normal drinking water or a high fat/high cholesterol diet with 10% fructose enriched drinking water. Biochemistry, histology and echocardiography analysis were performed to characterize NASH and HFpEF. Once the model was validated, elafibranor was evaluated at 15 mg/kg/day orally QD for 5 weeks.

*Results:* Hamsters fed a free choice diet for up to 20 weeks developed NASH, including hepatocyte ballooning (as confirmed with cytokeratin-18 immunostaining), bridging fibrosis, and a severe diastolic dysfunction with restrictive profile, but preserved ejection fraction. Elafibranor resolved NASH, with significant reduction in ballooning and fibrosis scores, and improved diastolic dysfunction with significant reduction in E/A and E/E′ ratios.

*Conclusion:* Our data demonstrate that the free choice diet induced NASH hamster model replicates the human phenotype and will be useful for validating novel drug candidates for the treatment of NASH and associated HFpEF.


## 1. Introduction

Physiological mechanisms favoring energy storage as fat in the liver (steatosis), blood (serum triglycerides) and white adipose tissue (adipocytes) in preparation for a period of food shortage are present in numerous animal species and humans [1]. This biological process, that includes a switch from lean-sensitive to obese insulin resistant state [2], enabled survival during food shortages in human evolution [3]. Over the last decades however, this survival advantage has turned to be highly problematic in the context of urbanization and constantly available energy-dense foods, with a dramatic increase in obesity prevalence worldwide [4]. Obesity is associated with several co-morbidities including insulin resistance, dyslipidemia, nonalcoholic fatty liver

*Abbreviations:* ALT, alanine aminotransferase; AST, aspartate aminotransferase; CK18, cytokeratin-18; EF, ejection fraction; FS, fractional shortening; HDL-cholesterol, high density lipoprotein cholesterol; H&E, Hematoxylin and Eosin; HFpEF, heart failure with preserved ejection fraction; IHC, immunohistochemistry; LV, left ventricle; NAFLD, nonalcoholic fatty liver disease; NASH, nonalcoholic steatohepatitis; ph-CFS, phenotypic composite fibrosis score; PPAR, peroxisome proliferator activated receptor; qFPs, quantitative fibrosis parameters; qPCR, quantitative polymerase chain reaction; SHH, sonic hedgehog.

* Corresponding author.
*E-mail address:* f.briand@physiogenex.com (F. Briand).

https://doi.org/10.1016/j.metabol.2021.154707

disease (NAFLD), chronic kidney disease, hypertension and atherosclerosis, leading to a higher cardiovascular risk and premature mortality [5]. Due to its tight positive correlation with obesity and type 2 diabetes, the prevalence of NAFLD is also increasing worldwide [6]. NAFLD includes a spectrum of disorders, ranging from nonalcoholic fatty liver (simple liver steatosis), to nonalcoholic steatohepatitis (NASH). NASH is associated with inflammatory infiltrates, hepatocyte ballooning and fibrosis, which brings an increasing the risk to reach the most severe stages, i.e. cirrhosis and hepatocellular carcinoma [7]. Although a cause–effect association has not yet been demonstrated, NAFLD is also associated with increased risk of cardiovascular events and functional cardiac abnormalities [8]. Hence, a higher prevalence of left ventricular diastolic dysfunction or heart failure with preserved ejection fraction (HFpEF) is observed in NAFLD patients [9,10]. Additionally, liver fibrosis has been shown to be associated with left ventricular diastolic dysfunction [11] and predicts mortality in patients with HFpEF [12]. Overall, there is accumulating evidence for a liver to heart axis, where patients with the most severe fatty liver have increased cardiovascular mortality [13], and cardiovascular disease is the leading cause of deaths in NAFLD patients [14].

Although lifestyle and diet changes remain the primary intervention, novel therapies targeting NASH are needed. Given the higher cardiovascular risk observed in NAFLD patients, an effective drug should also demonstrate cardiac benefits. As no therapy has been marketed yet, preclinical mouse and rat models of NASH and liver fibrosis are extensively used for drug development. However, none fully replicates the NASH phenotype observed in the clinic [15] nor integrates the cardiovascular component, i.e. HFpEF, for preclinical drug development. Interspecies differences limit the translation of data observed in rodents to the human context [16]. For example, hepatocyte ballooning, a key histopathological marker to define human NASH, has not been observed in mouse models [17]. Mice also produce beta-muricholic acid, a bile acid not present in humans and therefore they represent a weak model to investigate the known influence of bile acids on NAFLD progression [18,19]. To solve these limitations, we have recently established a nutritional hamster model which develops obesity, insulin resistance, dyslipidemia and features similar to human NASH and liver fibrosis, including hepatocyte ballooning [20]. Unlike mouse and rat, the Golden Syrian hamster lipoprotein metabolism is similar to humans [21] and does not synthesize muricholic acids from cholesterol. As in humans, hamsters have a bile acid profile consisting of mostly glycine and taurine conjugates of cholic and chenodeoxycholic acids, with lesser amounts of deoxycholate and lithocholate [22]. Due to these similarities, our nutritional hamster model shows the same dyslipidemic sides effect of obeticholic acid, a farnesoid X receptor agonist for the treatment of human NASH, i.e. higher LDL-cholesterol and lower HDL-cholesterol levels [20,23–25].

In the present study, we further investigated whether our nutritional NASH hamster model also develops HFpEF, and whether a therapy improving NASH and liver fibrosis would also demonstrate a cardiovascular benefit. To test this hypothesis, hamsters were treated with elafibranor, a dual peroxisome proliferator activated receptor (PPAR) $\alpha/\delta$ agonist evaluated in the clinic for the treatment of NASH [26].

## 2. Methods

### 2.1. Animals and diet

All animal protocols were reviewed and approved by the local (Comité régional d'éthique de Midi-Pyrénées) and national (Ministère de l'Enseignement Supérieur et de la Recherche) ethics committees (protocol number CEEA-122–2014-15). Three experiments were performed in the present study as described in Fig. S1. After a 5-day acclimation period, male Golden Syrian hamsters (Janvier Labs, France), 4-week old at the beginning of the study were fed for up to 20 weeks either a control chow diet (5.1% fat, 19.3% protein, 55.5% carbohydrates, from Safe Diets) with normal drinking water, or a free choice diet. As shown in Fig. S2, the free choice diet consists of a choice, within the same cage, between control diet with normal water or a high fat/high cholesterol diet (40.8% fat, 14.8% protein, 44.4% carbohydrates and 0.5% cholesterol from Safe Diets, France) with 10% fructose-enriched drinking water. The high fat/high cholesterol diet was a mixture of 55% control chow diet, 20% peanut butter paste (Skippy, Hormel Foods Corporation, Austin, MN, USA) and 25% hazelnut paste (Nustikao, Leclerc, Ivry-sur-Seine, France), with vegetable oils as fat source, as described previously [20].

Experiment#1 (Fig. S1A) was devised to evaluate the extent of NASH and cardiac dysfunction over 20 weeks of free choice diet. At 10, 15 and 20 weeks of diet, hamsters ($n = 6$ chow and n = 6 free choice hamsters per timepoint) underwent echocardiography measurements, as described below. After a 2-day recovery period, hamsters were fasted for 6 h and then bled by retro-orbital bleeding under isoflurane anesthesia for plasma isolation, euthanized and exsanguinated with saline prior to liver and heart collection. Liver and heart samples were used to measure gene expression and perform histology analysis.

In Experiment#2 (Fig. S1B), the effects of elafibranor at 15 mg/kg/day on NASH and liver fibrosis were evaluated in free choice fed hamsters. Since no dose was previously published in hamsters, the dose of 15 mg/kg was selected based on other published mouse and rat studies. Animals were randomized after 15 weeks of free choice diet into 2 treatment groups ($n = 9$ per group) based on plasma alanine aminotransferase (ALT), aspartate aminotransferase (AST), and total cholesterol levels. Hamsters were then kept on free choice diet and treated orally once a day (p.o. QD) with vehicle (0.1% Tween 80 and 1% carboxymethyl cellulose in 98.9% distilled water) or elafibranor (reference # BE163306 purchased from Carbosynth, Compton, UK) administered at 15 mg/kg p.o. QD for 5 weeks. The elafibranor formulation was initiated by grinding a precise quantity in a mortar along with a small volume of 0.1% Tween 80 and 1% carboxymethyl cellulose vehicle. The suspension was stirred continuously at room temperature with addition of vehicle to final volume to obtain a homogenous formulation.

At the end of the 5-week treatment period, hamsters fasted for 6 h were then bled for plasma isolation, euthanized, and exsanguinated with saline prior to liver collection. Plasma and liver samples were used to perform biochemical and liver histology analysis. In each treatment group, liver samples from 4 hamsters were used for fibrosis histology phenotype analysis, as described below.

In Experiment#3 (Fig. S1C), free choice fed hamsters were randomized after 15 weeks of free choice diet into 2 treatment groups ($n = 5$ per group) based on plasma ALT, AST, total cholesterol levels, and E/A ratio (an index of diastolic function), as determined by echocardiography. Hamsters were then kept on free choice diet and treated with vehicle p.o. QD or elafibranor 15 mg/kg p.o. QD for 5 weeks. At the end of the 5-week treatment period, hamsters underwent echocardiography measurements. After a 2-day recovery period, hamsters were fasted for 6 h and bled for plasma isolation, euthanized, and exsanguinated with saline prior to liver and heart collection. Liver and heart samples were used to measure gene expression and perform histology analysis.

### 2.2. Echocardiography

Echocardiography was performed under isoflurane anesthesia (1.5–2%) using a high-frequency 16-MHz linear transducer (VF16-5 probe, Siemens Healthineers) connected to an ultrasound system (Acuson NX3 Elite, Siemens Healthineers), as described previously [27]. Data acquisition was performed in 2D-, M-, and Doppler modes, from parasternal long- and short axis, as well as apical 4 chamber views. Left ventricle volumes, diameters and wall thicknesses were measured

using Compacs software (Siemens), and three cardiac cycles were averaged for each parameter.

The LV ejection fraction (EF) and fractional shortening (FS) were calculated with the following formulas:

$$EF\% = [\text{end}-\text{diastolic volume (EDV)}-\text{end}-\text{systolic volume}]/EDV \times 100$$

$$FS\% = (\text{left ventricle internal diameter in diastole (LVIDd)} - \text{left ventricle internal diameter in systole LVIDs})/LVIDd \times 100$$

Diastolic function was assessed by pulse-wave Doppler imaging of the mitral flow. Early (E) and late (A) peak transmitral flow velocity and, the isovolumic relaxation time (IVRT) and annular tissue velocity of the mitral valve (e′ and a′ peaks) were measured and E/A ratio, as well as E/E′ were calculated.

### 2.3. Biochemical analysis

Plasma biochemistry was performed by the Genotoul Anexplo platform in Toulouse, France. Plasma ALT and AST, total cholesterol, HDL-cholesterol and triglycerides were determined, using a Horiba Pentra 400 machine and related Pentra assay kits (Horiba France SAS, Longjumeau, France). Non-HDL-cholesterol were calculated by subtracting HDL-cholesterol from total cholesterol values. Colorimetric assay kits were used to assay hepatic total cholesterol, triglycerides and fatty acids (references # WCHO100, WTRIG1000 and W1W434-91795 from Sobioda, Montbonnot-Saint-Martin, France) from liver homogenate after lipid solubilization with deoxycholate, as described previously [28].

### 2.4. Histology analysis

Histology and immunohistochemistry analysis were performed by Sciempath Labo. Hematoxylin and Eosin (H&E) staining was performed according to four major steps for histopathological evaluation staining nuclei and cytoplasm. After a first step of deparaffinization/rehydration, sections were stained using Hematoxylin. Then three washings were performed, and sections were stained in 1% eosin solution before dehydration for mounting on slides.

Sirius red staining of liver and heart was performed according to four major steps for collagen analysis. After a first step of deparaffinization/rehydration, sections were stained using Sirius red solution. Then, sections were transferred to picric acid in aqueous solution before dehydration for mounting on slides.

Sections stained with H&E, Sirius red were evaluated and individually scored as described previously [20]. A blinded NAFLD scoring system (NAS) adapted from Kleiner et al. [29] with a total of four variables, were qualitatively assessed and ranked with a score, as follow: hepatocellular steatosis was scored as 0 (<5% of liver parenchyma), 1 (5–33%), 2 (33–66%), 3 (>66%); lobular inflammation was scored as 0 (no foci), 1 (<2 foci per 20× field), 2 (foci per 20× field), 3 (>4 foci per 20× field); hepatocyte ballooning was scored as 0 (none), 1 (minimal to mild focal involving fewer than 3 hepatocytes per foci), 2 (moderate multifocal involving more than 3 hepatocytes per foci), 3 (prominent multifocal involving large number of hepatocytes); lobular fibrosis was scored as 0 (none), 1 (perisinusoidal or periportal), 2 (perisinusoidal and periportal), 3 (bridging fibrosis), 4 (cirrhosis). Total NAFLD activity score was then calculated for each animal by the sum of scores.

Hepatic histomorphometric measurements of positive area for Sirius red were performed using computer-assisted image analysis on individualized frames captured from digitized sections. In brief, the histomorphometric measurements were generated with the software Image Pro Premier (v. 9.2) from Media Cybernetics (Maryland, USA) using a semi-automated approach. A slight gamma, RGB and contrast correction on each section was used to enhance the positive Sirius red staining from the rest of the lobular components in order to facilitate the segmentation of positive staining without affecting the morphometric measurements since these didn't contain data based on intensity. Fields were selected at 5× magnification for morphometric evaluation. Field selection was made with care to exclude possible overlap between images and the total surface analyzed in each section represented >95% of the total surface of each lobe present on histological slides. Each selected field was saved as a JPEG single image. The pixel value at 5× magnification corresponded to 1.82 μm/pixel. An algorithm was generated for Sirius Red morphometric measurement on liver-stained sections. The algorithm was generated with the smart segmentation tool in the software package, which was further refined through training on a subset of twenty-five images from 5 animals. Sirius red positive area from major centri-lobular and portal blood vessels, as well as capsular connective stroma, was manually dissected and removed from detected positive area. For each analyzed image, all detected positive pixels were summed and used to determine total area analyzed ($pixel^2$), total positive area ($pixel^2$) and % "positive" area/area analyzed (%).

Myocardial whole-section histomorphometric measurements of positive area for Sirius red were performed using computer assisted image analysis on digitized sections. In brief, the histomorphometric measurements were generated with the software from Visiopharm (Denmark) using an automated approach. Analysis was performed on virtual whole sections at 20× magnification for morphometric evaluation. An algorithm was prepared for Sirius red morphometric measurement on heart-stained sections. The algorithm was generated with the Bayesian linear segmentation tool in the software package, which was further refined through training on a subset of sections from 5 animals. Major histology section artefacts, coronary vessel, as well as large empty interstitial space were automatically or manually dissected and removed from area of interest (AOI) or detected positive area. As for the liver, all detected positive pixels were summed and used to determine total myocardial area analyzed or AOI ($mm^2$), total Sirius red positive area ($mm^2$), % Sirius red area/total area analyzed (%).

For immunohistochemistry, livers samples were embedded in paraffin for microtome sectioning at 4 μm. Sections were deparaffinized, then incubated in antigen retrieval solution at 97 °C for 20 min in a water bath (PT-Link). Sections were transferred to the autostainer (AutostainerLink48, Dako) at room temperature. First, an endogenous peroxidase blocking solution was added on sections twice for 5 min. This step was followed by a protein block for 10 min. Sections were incubated 1 h with the primary antibody at room temperature (RT). Primary antibodies used in this study were: rabbit anti-α-SMA (Abcam reference # ab5694, 1:500); rabbit anti-Ck18 (Invitrogen reference MA-14479, 1:15); rabbit anti-Collagen III (Bio-Rad reference AHP 1848, 1:200); rabbit anti-SHH (LSBio reference LS-C40460, 1:25). After washings, sections were incubated with the EnVision/HRP rabbit (K4003, Agilent) DAB (K3468, Agilent) revealing solution and finally counter-stained with hematoxylin (K8008, Agilent).

### 2.5. Fibrosis histology phenotype analysis

Quantification of fibrosis histology phenotype was performed by PharmaNest. Liver histology sections stained with Sirius Red (with no Hematoxylin staining) were imaged with light microscopy at 20×. We used FibroNest™ (PharmaNest, Princeton, USA), a cloud-based image analysis platform, to quantify the fibrosis histology phenotype expressed in the digital images. Three complimentary phenotypic layers are quantified including high level Collagen signatures (12 traits, including Collagen Proportion area, Collagen Reticulation Index, and Assembled/Fine Collagen), Morphometric signatures for each individual fiber (13 traits, including Fiber length, width, area, and perimeter and texture, i.e. relative arrangement or architecture of the fibers). Each trait is described by several quantitative fibrosis parameters (qFPs) to account for mean, variance, distortion, and progression. Fine and

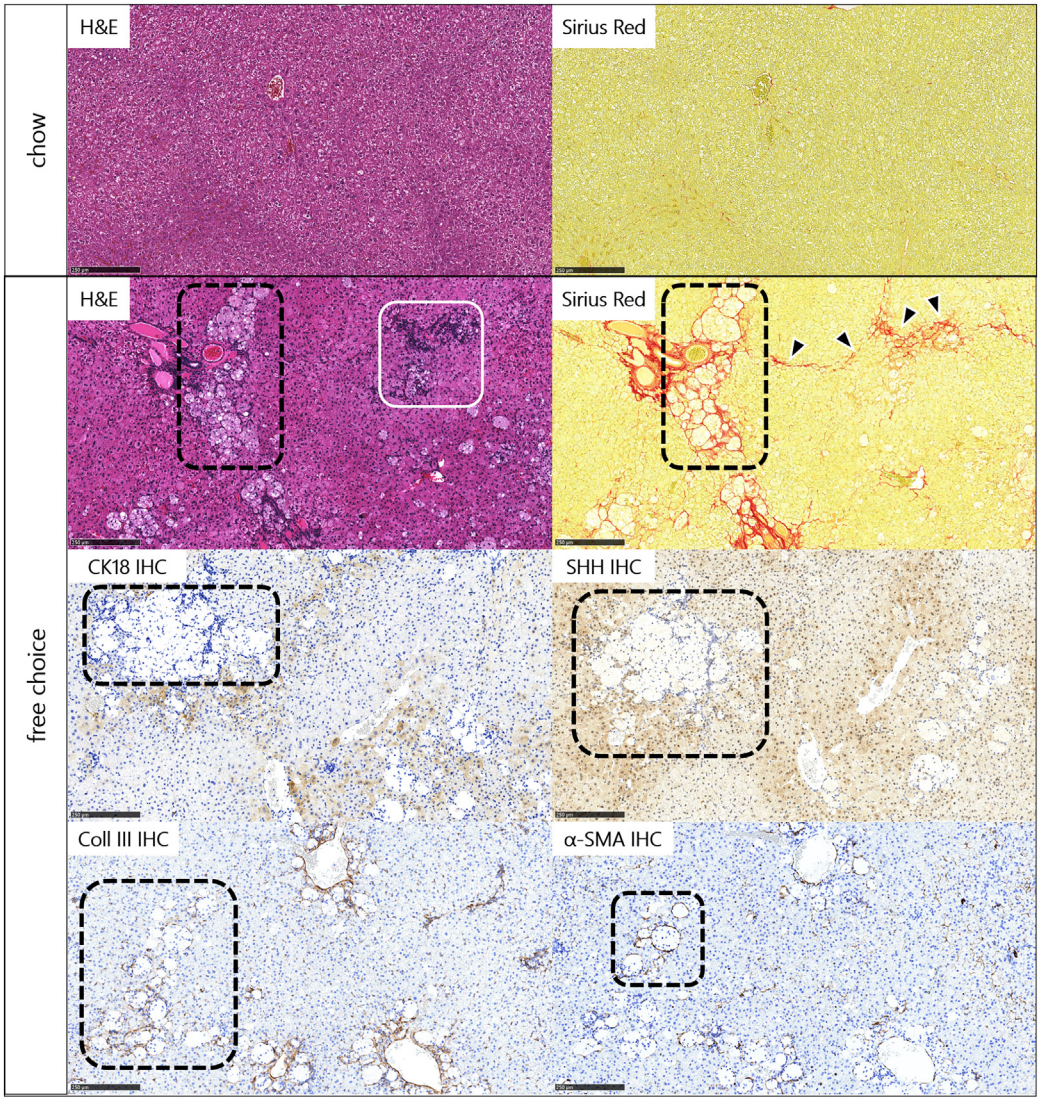
chow
free choice
H&E
Sirius Red
H&E
Sirius Red
CK18 IHC
SHH IHC
Coll III IHC
α-SMA IHC

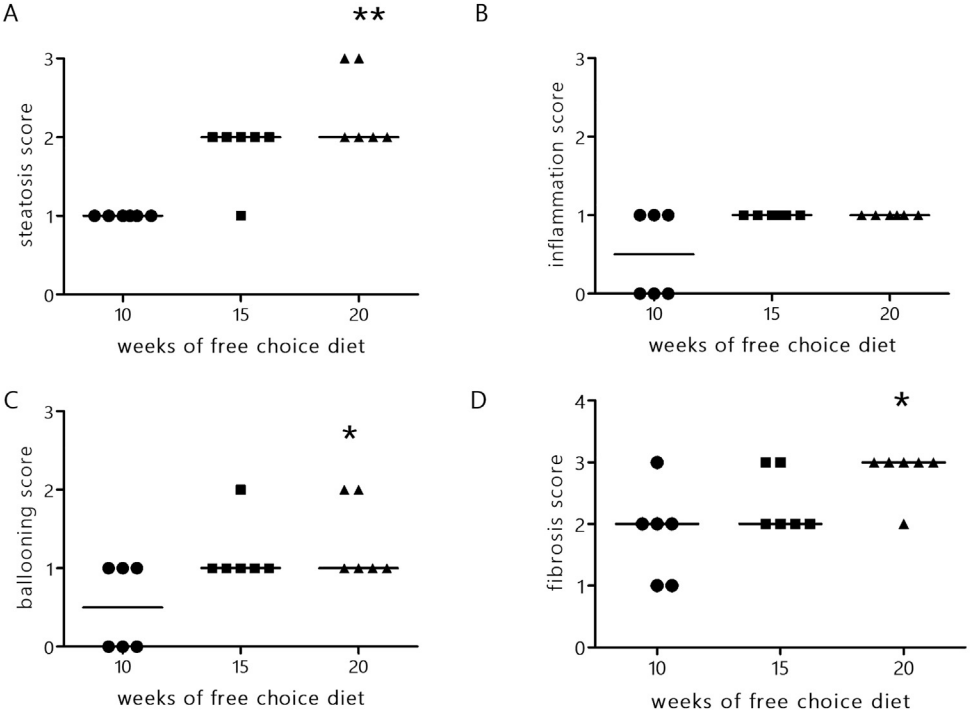
A
**
steatosis score
weeks of free choice diet
B
inflammation score
weeks of free choice diet
C
*
ballooning score
weeks of free choice diet
D
*
fibrosis score
weeks of free choice diet

Assembled collagen fibers are segregated into two sub-classes that are similarly quantified, to provide additional insights on the generation, coalescence, and progression of the fibrosis structures. Out of the ~350qFPs generated, a reduced group of ~80 principal qFPs are automatically selected to account for variance and optimize signal-to-noise. The principal qPFs are combined to generate a Phenotypic Composite Fibrosis Score (ph-CFS), a continuous phenotypic quantifier of fibrosis. The ph-CFS can be established for each subgroup of traits (e.g. Morphometric phenotype, or texture only phenotype) to provide additional insights on mechanisms of action in the progression or regression of fibrosis.

### 2.6. Gene expression analysis

Gene expression analysis was performed at the Neurocentre Magendie. Liver and heart tissues samples were homogenized in Tri-reagent (Euromedex, France) and RNA was isolated using a standard chloroform/isopropanol protocol [30]. RNA was processed and analyzed following an adaptation of published methods [31]. cDNA was synthesized from 2 μg of total RNA using Maxima Reverse Transcriptase (Thermoscientific) and primed with oligo-dT primers (Thermoscientific) and random primers (Thermoscientific). QPCR was performed using a LightCycler® 480 Real-Time PCR System (Roche, Meylan, France). QPCR reactions were done in duplicate for each sample, using transcript-specific primers, cDNA (4 ng) and LightCycler 480 SYBR Green I Master (Roche) in a final volume of 10 μl. The PCR data were exported and analyzed in an informatics tool (Gene Expression Analysis Software Environment) developed at the NeuroCentre Magendie. For the determination of the reference gene, the Genorm method was used. Relative expression analysis was corrected for PCR efficiency and normalized against two reference genes. The glucuronidase beta (Gusb) and Actin beta (Actb) genes were used as reference genes for liver. The ribosomal protein L37 (Rpl37) and succinate dehydrogenase flavoprotein subunit A (Sdha) genes were used as reference genes for heart. The relative level of expression was calculated using the comparative ($2^{-\Delta\Delta CT}$) method [32]. Primers sequences are reported in Table S1.

### 2.7. Statistical analysis

Data are presented as mean ± S.E.M. Ordinal data (i.e. steatosis, inflammation, ballooning, fibrosis and total NAFLD activity scores) are presented as median. Unpaired 2-tailed Student's *t*-test, Mann-Whitney, or Kruskal-Wallis + Dunn's post-test test were used for statistical analysis using GraphPad Prism software (GraphPad Software, La Jolla, CA, USA). A $P < 0.05$ was considered significant.

## 3. Results

### 3.1. Free choice diet promotes NASH, liver fibrosis and heart failure with preserved ejection fraction in hamsters

In Experiment#1, we investigated whether free choice diet from 10 to 20 weeks promotes both NASH and HFpEF in hamsters. Liver lesions were absent or limited to residual collagen deposition in chow fed hamsters (see representative H&E and Sirius Red staining in Fig. 1). Hamsters fed the free choice diet for 20 weeks presented a marked pan-lobular micro-vesicular steatosis, accompanied by hepatocellular ballooning and degeneration, which was associated with a discrete to mild mixed inflammatory reaction surrounding ballooned hepatocytes (see H&E staining in Fig. 1). Peri-sinusoidal, peri-portal and bridging fibrosis was also observed (see Sirius Red staining in Fig. 1). To demonstrate the presence of hepatocyte ballooning in hamsters, immunohistochemistry (IHC) for cytokeratin-18 (CK18) and sonic hedgehog (SHH) was performed. A very strong and specific IHC signal for CK18 was observed in hepatocytes localized in acinar Zone-1 and Zone-2, and to a lesser degree in Zone-3. Importantly, CK18 expression was completely lost in ballooned hepatocytes, when compared to normal adjacent hepatocytes (see CK18 IHC in Fig. 1). A very strong signal for SHH was observed in endothelial cells and mononuclear inflammatory cells in areas with inflammation. The signal in those cells was both cytoplasmic and nuclear. SHH expression was especially strong in mononuclear cells surrounding ballooned hepatocytes (see SHH IHC in Fig. 1). Additionally, further IHC analysis showed collagen III and alpha-SMA immunostaining signal surrounding ballooned hepatocytes (see coll III and α-SMA IHC in Fig. 1).

To confirm the induction of NASH and liver fibrosis during the 10 to 20 weeks free choice diet period, NAFLD activity scoring was performed in free choice fed hamsters (chow fed hamsters were not scored due to the lack of liver lesions, as described previously in this hamster model [20]). Steatosis score gradually increased during the diet leading to significantly higher score at 20 weeks versus 10 weeks (Fig. 1A). Inflammation score rapidly reached a plateau of score 1 at 15 weeks of diet (Fig. 1B), while hepatocyte ballooning tended to worsen significantly at 20 weeks of diet (Fig. 1C). Fibrosis score (Fig. 1D) also increased significantly from a score 2 (portal fibrosis) at 10 weeks to a score 3 (bridging fibrosis) at 20 weeks of diet.

To evaluate whether the free choice diet induces HFpEF, echocardiography was performed at 10, 15 and 20 weeks of diet (see complete echocardiography data in Table S2 and representative echocardiography pictures in Fig. S3). At 10 weeks of diet, similar ejection fraction (Fig. 2A) was observed between chow fed and free choice fed hamsters. As shown in Fig. 2B and Table S2, both ratios of peak velocities of early to late mitral inflow (E/A) and of mitral annular velocities (E′/A′), were significantly decreased but not reversed ($P < 0.05$). The E/E′ ratio, a marker of left ventricular filling pressure, remained unchanged at 10 weeks of diet, as compared with chow fed hamsters (Fig. 2C). At 15 weeks of diet, ejection fraction remained preserved in free choice fed hamsters (see Fig. 2D), but E/A ratio (Fig. 2E) was found significantly higher ($P < 0.01$ vs. chow), and E′/A′ ratio significantly reversed (Table S2). In addition, E/E′ ratio (Fig. 2F) was higher, although it did not reach significance. At 20 weeks, ejection fraction was still preserved in free choice fed hamsters (Fig. 2G). The E/A ratio (Fig. 2H) was further increased with a concomitant inverted E′/A′ ratio (Table S2), both significantly, indicating a restrictive filling pattern. Similarly, the significantly higher E/E′ ratio (Fig. 2I) suggested an elevated left atrial pressure. Altogether, these results indicate a model of progressive diastolic dysfunction leading to an impairment of left ventricular compliance. Additionally, histology analysis of heart samples also highlighted cardiac fibrosis (Fig. 2J), with a higher % Sirius Red labelling after 20 weeks of free choice diet ($P < 0.05$ vs. chow).

Overall, the present data indicate that 15 to 20 weeks of free choice diet induces substantial liver lesions, including hepatocyte ballooning and bridging fibrosis. The free choice diet-induced NASH is also associated with HFpEF, characterized by a severe diastolic dysfunction with restrictive profile (ultimate grade III), while ejection fraction remains unaffected.

**Fig. 1.** Free choice diet for 20 weeks induces NASH and liver fibrosis in hamsters. Upper panel shows representative histology pictures for H&E, Sirius Red, cytokeratin-18 (CK18) and Sonic HedgeHog (SHH), collagen III (coll III) and α-SMA immunohistochemistry (IHC) in control chow and free choice fed hamsters. Dashed black squares indicate clusters of ballooned hepatocytes surrounded by fibrosis with loss of CK18 and surrounded by cells expressing SHH or collagen III and α-SMA brown signal, white square indicates inflammatory foci and black arrows indicate bridging fibrosis. Histopathological scoring for steatosis (A), inflammation (B), ballooning (C) and fibrosis (D) at 10, 15 and 20 weeks of free choice diet. Ordinal data are shown as median. Statistical analysis was performed using a Kruskal-Wallis + Dunn's post-test. $^{*}P < 0.05$ and $^{**}P < 0.01$ 20 weeks vs. 10 weeks of diet, $n = 6$ per group.

### 3.2. Free choice diet alters the expression of genes involved in lipid metabolism, inflammation, and fibrosis in both the liver and heart

To further characterize the hepatic and cardiac alterations induced by the free choice diet, hepatic expression of genes involved in bile acids and lipid metabolism, inflammation, and fibrosis was measured in both the liver and heart at 20 weeks of diet. Compared to chow fed hamsters, liver gene expression of Cyp7a1 (Fig. 3A) and Cpt1a (Fig. 3B) was significantly reduced by 70% and 40%, respectively, in free choice fed hamsters. A 79% lower expression was observed for the LDL-receptor (Fig. 3C) gene ($P < 0.01$ vs. chow) while ABCG5 (Fig. 3D) gene expression was 2.5-fold high ($P < 0.001$ vs. chow). As expected, hepatic expression of genes involved in inflammation, i.e. TNF-α (Fig. 3E), IL-1β (Fig. 3F) and IL-6 (Fig. 3G) were significantly higher by 4-, 2- and 4-fold, respectively (all $P < 0.01$ vs. chow). In line with the fibrosis score, collagen 1α1 (Fig. 3H) was 7-fold higher in free choice fed hamster ($P < 0.01$ vs. chow). Alteration of genes expression by free choice diet was not as pronounced in the heart, although the expression of FAS (Fig. 3I), Srebp-1c (Fig. 3J) and UCP2 (Fig. 3K) genes were significantly higher by approximately 1.3-fold vs. chow diet. In line with the higher cardiac collagen deposition observed in free choice fed hamsters, a small but significant increase (1.2-fold, $P < 0.05$ vs. chow) was observed in the expression of TGF-β (Fig. 3L).

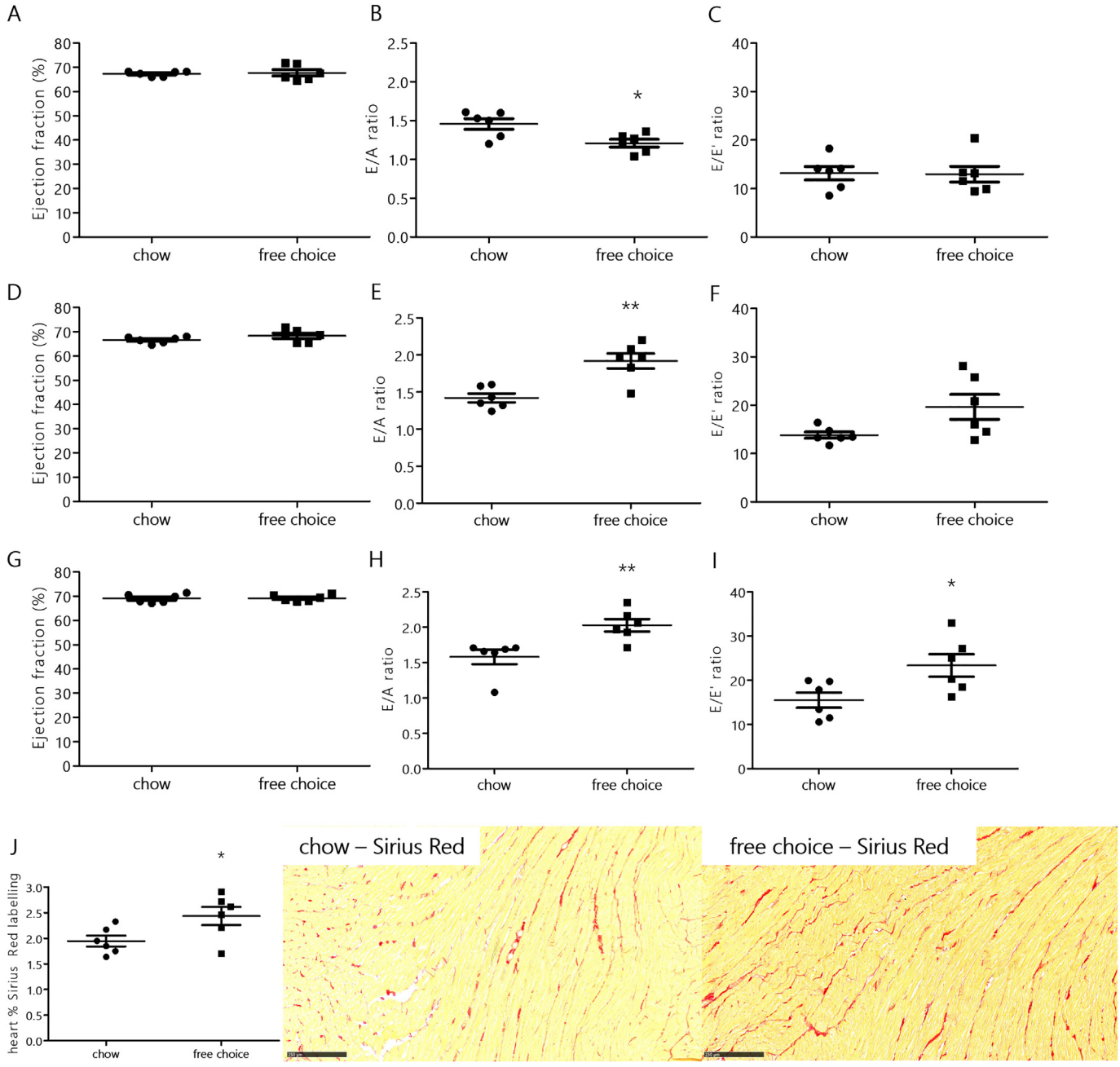


**Fig. 2.** Free choice diet for 20 weeks induces heart failure with preserved ejection fraction in hamsters. Echocardiography was performed at 10 weeks (A–C), 15 weeks (D–F) and 20 weeks (G–I) in hamsters fed a control chow or free choice diet, to measure several parameters including ejection fraction (A, D, G), E/A ratio (B, E, H) and E/E′ ratio (C, F, I). Heart histology analysis (Sirius Red) was performed at 20 weeks of diet in chow and free choice fed hamsters to quantify % Sirius Red labelling (J). Data are shown as mean ± SEM. Statistical analysis was performed using an unpaired two-tailed Student's *t*-test or a Mann-Whitney test. $^{*}P < 0.05$ and $^{**}P < 0.01$ chow vs. free choice, n = 6 per group.

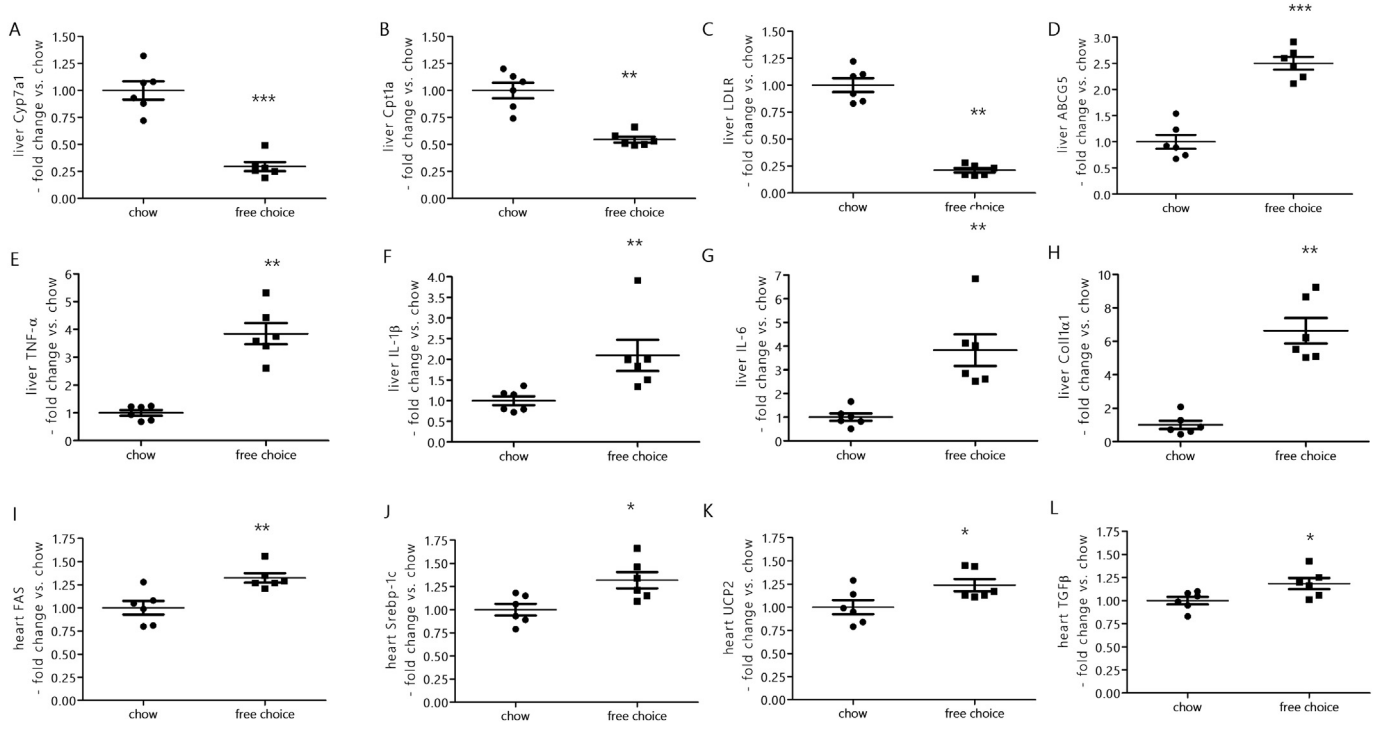


**Fig. 3.** Free choice diet for 20 weeks alters hepatic and cardiac gene expression. Expression of hepatic Cyp7a1 (A), Cpt1a (B), LDLR (C), ABCG5 (D), TNF-α (E), IL-1β (F), IL-6 (G), coll1α1 (H), cardiac FAS (I), Srebp-1C (J), UCP2 (K) and TGF-β (L) was measured by RT-qPCR. Data are shown as mean ± SEM. Statistical analysis was performed using an unpaired two-tailed Student's *t*-test or a Mann-Whitney test. $^{*}P < 0.05$, $^{**}P < 0.01$ and $^{***}P < 0.001$ free choice vs chow, n = 6 per group.

### 3.3. Elafibranor improves NASH and liver fibrosis in free choice fed hamsters

In Experiment#2, we evaluated whether intervention with dual PPAR α/δ agonist elafibranor 15 mg/kg/kg for 5 weeks would result in significant NASH and fibrosis resolution in 15-week free choice fed hamsters. Compared with vehicle, elafibranor tended to lower body weight at the end of the 5-week treatment period, but not significantly (Table 1). A 48% reduction in plasma ALT levels was observed in elafibranor treated hamsters ($P < 0.01$ vs. vehicle). Although plasma total cholesterol levels were reduced by 16% with elafibranor ($P < 0.05$ vs. vehicle), no significant change was observed in plasma HDL-cholesterol, non-HDL-cholesterol or triglycerides levels (Table 1). In addition, hepatic total cholesterol and fatty acids levels remained unchanged, but liver triglycerides levels were reduced by 42% in elafibranor treated hamsters ($P < 0.01$ vs. vehicle).

**Table 1**
Biochemical parameters in free choice fed hamsters treated with vehicle or elafibranor 15 mg/kg orally QD for 5 weeks.

| Parameter | Vehicle | Elafibranor |
|---|---|---|
| Body weight (g) | 165 ± 6 | 147 ± 6 |
| Plasma ALT (U/L) | 133 ± 20 | 69 ± 3** |
| Plasma AST (U/L) | 56 ± 5 | 51 ± 3 |
| Plasma total cholesterol (g/L) | 3.03 ± 0.15 | 2.55 ± 0.17* |
| Plasma HDL-cholesterol (g/L) | 2.07 ± 0.17 | 1.86 ± 0.17 |
| Plasma non-HDL-cholesterol (g/L) | 0.96 ± 0.14 | 0.68 ± 0.12 |
| Plasma triglycerides (g/L) | 2.80 ± 0.25 | 2.82 ± 0.22 |
| Hepatic total cholesterol (mg/g liver) | 106 ± 6 | 107 ± 6 |
| Hepatic triglycerides (mg/g liver) | 24 ± 2 | 14 ± 2** |
| Hepatic fatty acids (μmol/g liver) | 61 ± 2 | 59 ± 1 |

Data are shown as mean ± S.E.M., n = 9 hamsters per group. Statistical analysis was performed using an unpaired 2-tailed Student's *t*-test or a Mann-Whitney test.
* $P < 0.05$.
** $P < 0.01$ elafibranor vs. vehicle.

Histology analysis was performed to evaluate the effects of elafibranor on NASH and liver fibrosis. As expected, free choice hamsters treated with vehicle showed extended liver lesions with microvesicular steatosis, inflammation (see representative H&E staining in Fig. 4), bridging fibrosis and collagen deposition around ballooned hepatocytes (see Sirius Red staining in Fig. 4), with typical expression patterns for CK18 and SHH (see CK18 and SHH IHC in Fig. 4G). In contrast, treatment with elafibranor in free choice hamsters resulted in substantial improvement of liver lesions (see representative pictures in Fig. 4). These benefits were confirmed with NAFLD activity scoring indicating lower steatosis (Fig. 4A), inflammation (Fig. 4B), ballooning (Fig. 4C) and fibrosis (Fig. 4D) scores. To further characterize the anti-fibrotic effect of elafibranor, automated fibrosis quantification was performed. As shown in Fig. 5, elafibranor treatment resulted in substantially lower collagen liver content. Accordingly, elafibranor significantly reduced phenotypic (Fig. 5A) and bulk (Fig. 5B) collagen fibrosis scores (both $P < 0.05$ vs. vehicle), while morphometric (Fig. 5C) and texture (Fig. 5D) scores remained unaltered. This shows that elafibranor reduction in Phenotypic Fibrosis Score (ph-CFS) was due to liver collagen fibrosis measurements (contributed by collagen area, density, reticulation index, assembled/fine collagen), rather than either the Fibrosis Texture or the Morphometric aspect of the collagen fibers.

### 3.4. Elafibranor improves both NASH and liver fibrosis and heart failure with preserved ejection fraction in free choice fed hamsters

In Experiment#3, we investigated whether the benefits of elafibranor on NASH and liver fibrosis could also result in an improved cardiac function in free choice fed hamsters. Potential target genes of elafibranor that are involved in bile acids synthesis and lipid metabolism, inflammation and fibrosis were selected for hepatic gene expression. Elafibranor significantly changed the gene expression of hepatic Cyp7a1 (Fig. 6A), Cpt1a (Fig. 6B), ABCG5 (Fig. 6C), TNF-α (Fig. 6D), IL-1β (Fig. 6E) and collagen 1α1 (Fig. 6F). However, no significant change

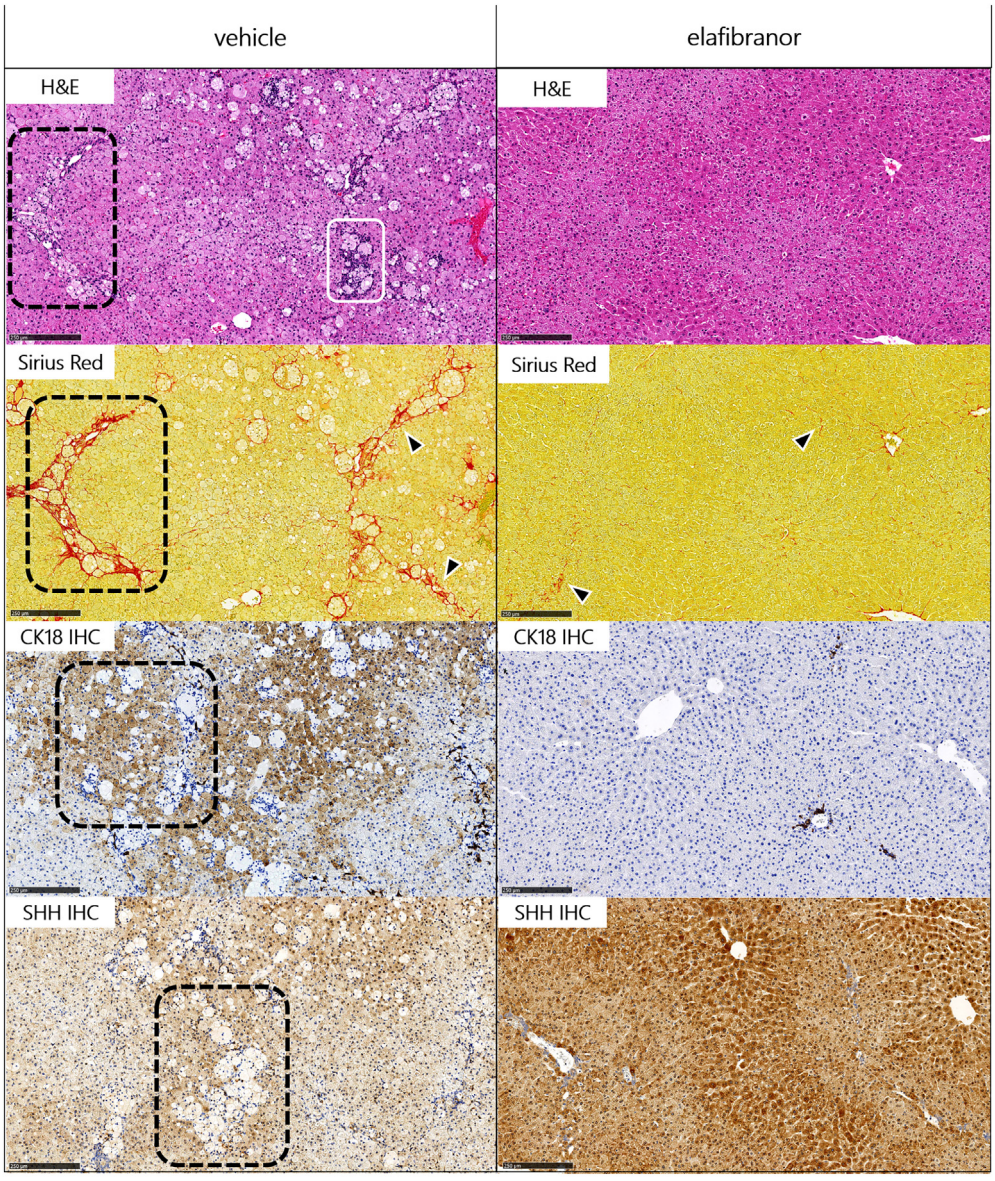
vehicle
elafibranor
H&E
H&E
Sirius Red
Sirius Red
CK18 IHC
CK18 IHC
SHH IHC
SHH IHC

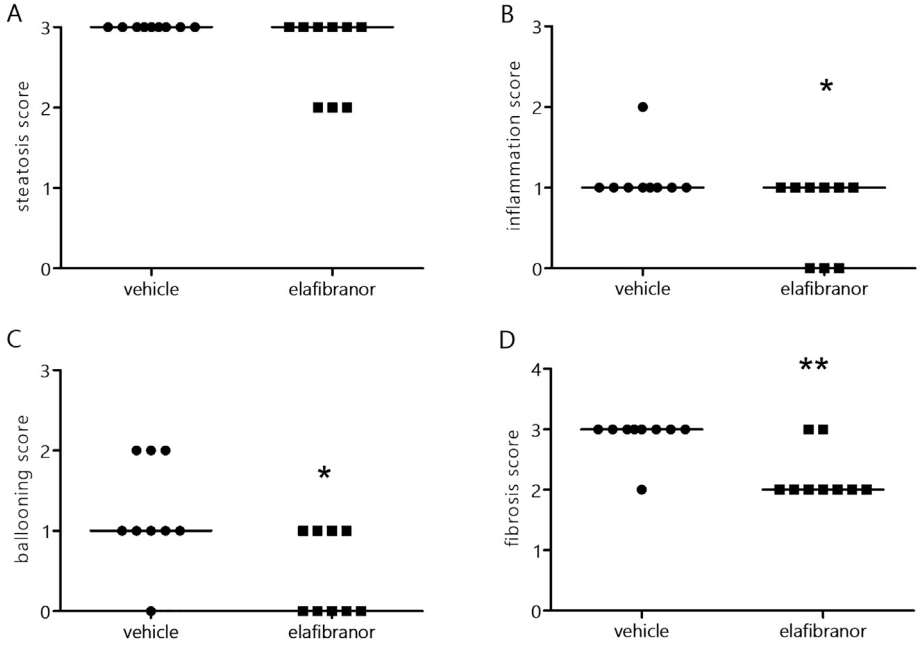
A
steatosis score
0
1
2
3
vehicle
elafibranor
B
inflammation score
*
C
ballooning score
*
D
fibrosis score
**

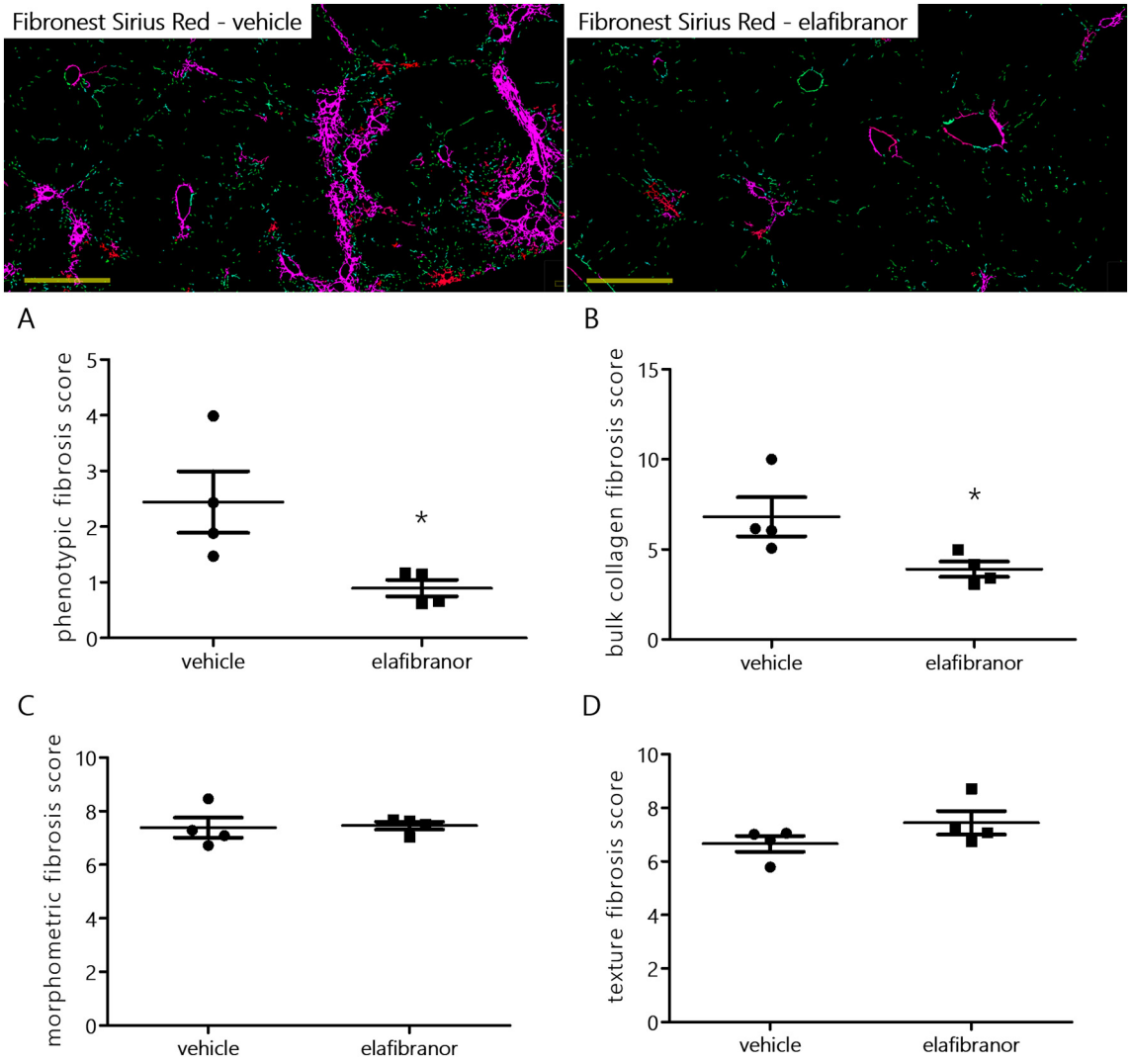


**Fig. 5.** Elafibranor improves fibrosis histology phenotype. Upper panel shows representative pictures from Viqi Software (yellow bar indicates 500 μm scale) of FibroNest Sirius Red analysis in free choice hamsters treated with vehicle and elafibranor from which phenotypic (A), bulk collagen (B), morphometric (C) and texture (D) scores were calculated. Fine Collagen (green). Assembled Collagen (magenta) is the highly reticulated collagen fibers. Data are shown as mean ± SEM. Statistical analysis was performed using an unpaired two-tailed Student's *t*-test. $^{*}P < 0.05$ elafibranor vs. vehicle, $n = 4$ per group.

in gene expression was observed in the heart (data not shown). As expected, elafibranor showed significant benefits on liver lesions, with lower collagen deposition (see % Sirius Red labelling in Fig. 6G), steatosis score (Fig. 6H), inflammation score (Fig. 6I), ballooning score (Fig. 6J) and fibrosis score (Fig. 6K), leading to a significant reduction in the total NAFLD activity score (Fig. 6L).

At the end of the treatment period, echocardiography was also performed (see complete echocardiography data in Table S3 and representative echocardiography pictures in Fig. S3). In parallel with the significant improvement in NASH and liver fibrosis, elafibranor showed evidence of cardiac benefits. Without impacting systolic function and ejection fraction (Fig. 6M), elafibranor significantly improved diastolic dysfunction and filling pressure as evidenced by reduced E/A (Fig. 6N) and E/E′ (Fig. 6O) ratios, and increased E′/A′ ratio (Table S3). However, cardiac collagen content as measured with % Sirius Red staining remained unchanged (vehicle: 2.4 ± 0.2%; elafibranor: 2.2 ± 0.1%).

The present data indicate that improvement of NASH and liver fibrosis by elafibranor also results in cardiac benefits with improved left ventricular diastolic dysfunction in free choice fed hamsters.

## 4. Discussion

We have previously described that free choice diet induced obesity, dyslipidemia, NASH and liver fibrosis in the Golden Syrian hamster [20]. While similar metabolic disorders were again observed, the present study further characterized hepatocyte ballooning with an immunostaining approach and demonstrated that free choice diet in hamsters induced progressive liver lesions and diastolic dysfunction. As

**Fig. 4.** Elafibranor improves NASH and liver fibrosis in free choice fed hamsters. Upper panel shows representative histology pictures for H&E, Sirius Red, cytokeratin-18 (CK18) and Sonic HedgeHog (SHH) immunohistochemistry (IHC) in free choice fed hamsters treated with vehicle or elafibranor. Dashed black squares indicate clusters of ballooned hepatocytes surrounded by fibrosis with loss of CK18 and surrounded by cells expressing SHH brown signal, white square indicates inflammatory foci and black arrows indicate bridging fibrosis. Dashed black squares indicate ballooned hepatocytes with loss of CK18 and surrounded by cells expressing SHH. Histopathological scoring for steatosis (A), inflammation (B), ballooning (C) and fibrosis (D) in free choice fed hamsters treated with vehicle or elafibranor. Ordinal data are shown as median. Statistical analysis was performed using an unpaired two-tailed *t*-test. $^{*}P < 0.05$ and $^{**}P < 0.01$ elafibranor vs. vehicle, $n = 9$ per group.

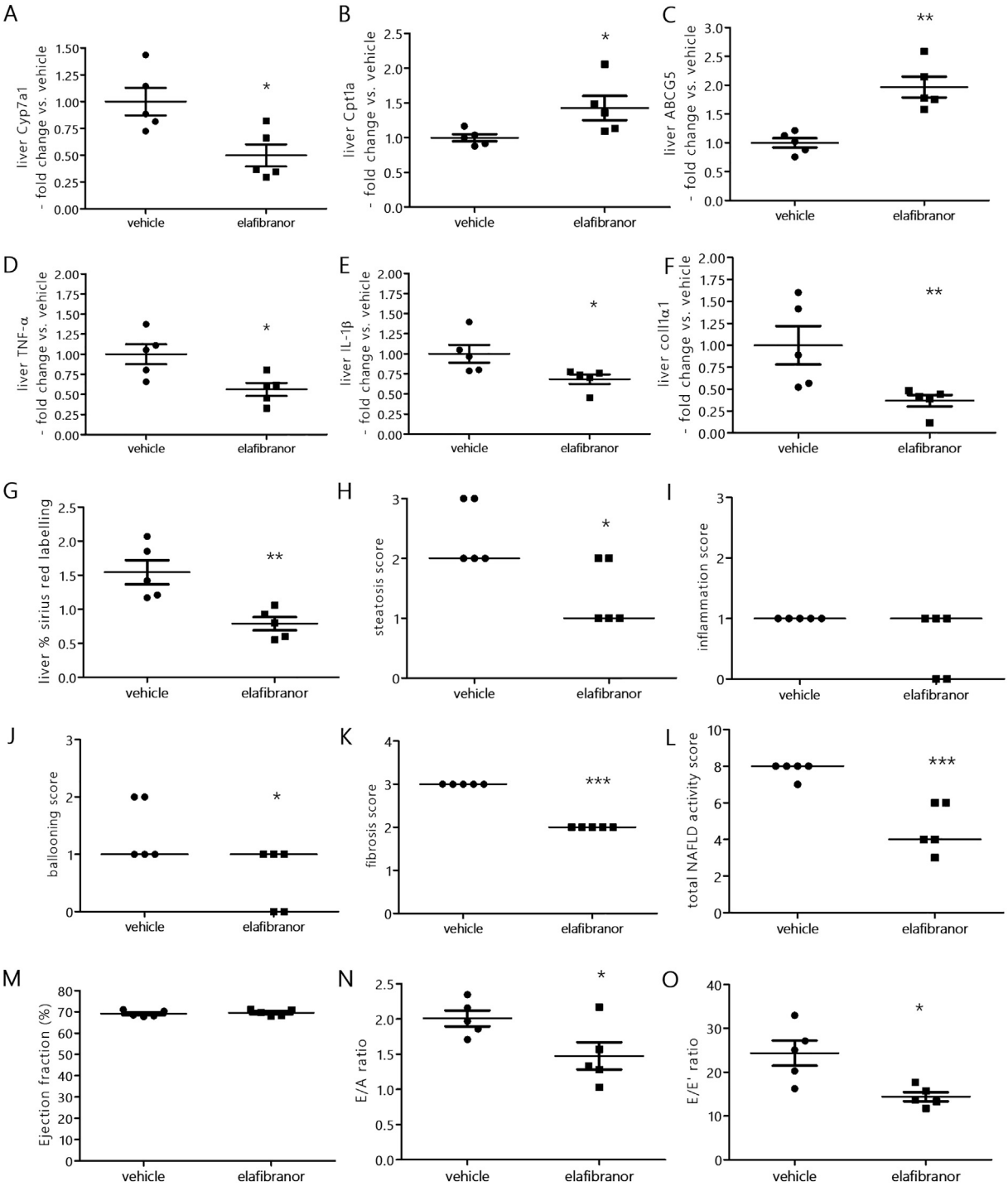


**Fig. 6.** Elafibranor improves both NASH and HFpEF in free choice fed hamsters. Expression of hepatic Cyp7a1 (A), Cpt1a (B), ABCG5 (C), TNF-α (D), IL-1β (E), coll1α1 (F), was measured by RT-qPCR. Histology analysis was used to quantify % Sirius Red labelling (G) and perform steatosis (H), inflammation (I), ballooning (J), fibrosis (K) and total NAFLD activity scores (L). Echocardiography was performed to measure ejection fraction (M), E/A (N) and E/E′ (O) ratios. Data are shown as mean ± SEM. Ordinal data from histology scoring (panels H–L) are shown as median. Statistical analysis was performed using an unpaired two-tailed Student's *t*-test. $^{*}P < 0.05$, $^{**}P < 0.01$ and $^{***}P < 0.001$ elafibranor vs. vehicle, $n = 5$ per group.

cardiovascular disease is the leading cause of death in patients with NAFLD, we hereby provide a preclinical model to evaluate novel therapies on both NASH and HFpEF.

To our knowledge, only one preclinical study investigated the organ interaction between NASH and cardiac dysfunction in stroke-prone spontaneously hypertensive SHRSP5/Dmcr rats [33]. In association with NASH and hypertension, this rat fed a high fat/high cholesterol diet developed cardiac and vascular dysfunction with cardiac fibrosis, endothelial dysfunction, and moderate left ventricular diastolic dysfunction. Although these findings are in the same line as the data observed in our hamster study, NAFLD activity and fibrosis scores were not performed and diastolic dysfunction was in the early stage, as shown by the increase in isovolumic relaxation time and deceleration time. It is not known whether a drug improving NASH would also reverse cardiac dysfunction in this rat model. Importantly, the rat model also has limitations with regard to its different lipoprotein cholesterol metabolism compared to humans. For instance, the dyslipidemic side effect of obeticholic acid raising LDL-cholesterol observed in humans could not

be detected in rats [23]. Moreover, the rat profile of bile acids, which play a crucial role in NAFLD progression [19], is clearly dissimilar to humans [34]. Mice also present a very different bile acids profile in comparison to humans [18] but are widely used as nutritional or genetic NASH models for preclinical development [15]. Among those models, leptin deficient ob/ob mice exhibit liver steatosis associated with cardiac dysfunction [35], but this includes a reduced ejection fraction, which differs from the human context of HFpEF associated with NASH and liver fibrosis. Another limitation of NASH mouse models, except for those with genetically induced keratin-18 deficiency, is the lack of evident hepatocyte ballooning [17] for scoring this key NASH histopathological marker. As already observed in other hamster studies [20,36], we have further demonstrated the presence of hepatocyte ballooning in diet-induced NASH hamsters, with the loss of CK18 immunostaining, an objective marker of ballooning degeneration of hepatocytes in NASH [37]. Interestingly, ballooned hepatocytes are also surrounded by SHH, a ligand of hedgehog which induces hepatic stellate cells activation and its marker α-SMA, and liver fibrogenesis [38]. Accordingly, immunostaining for both α-SMA and collagen III was also evident around these ballooned hepatocytes. In contrast to the limitations of mouse and rat, these histological observations indicate that the free choice hamster is a robust NASH model to evaluate the effects of drugs on hepatocyte ballooning.

Since nuclear receptors PPAR play a regulatory role in lipid metabolism and inflammation, which are important factors in NASH, the dual PPARα/δ agonist elafibranor has been developed for the treatment of NASH [39]. In chemical, nutritional, and transgenic animal models of NASH/liver fibrosis, elafibranor has shown liver-protective effects on steatosis, inflammation, and fibrosis, as well as inhibition of proinflammatory (i.e. TNF-α, IL-1β) and profibrotic (i.e. coll1α1) gene expression [40]. Elafibranor showed the same benefits in free choice hamsters, with reduction in NAFLD activity scoring and liver fibrosis, as well as lower expression of the same genes involved in inflammation (i.e. TNF-α, IL-1β) and fibrosis (coll1α1). In the GOLDEN-505 study, elafibranor significantly improved dyslipidemia, hepatocyte ballooning and lobular inflammation with a trend toward improvement in steatosis in patients with NASH [39]. Patients with NASH resolution after receiving elafibranor also had significantly reduced liver fibrosis stages in this phase II clinical trial. Although the anti-dyslipidemic effects of elafibranor were limited to significant reduction of cholesterolemia, similar hepatic benefits were observed in free choice hamsters, including lower fibrosis score and occasional individuals showing complete resolution of hepatocyte ballooning and inflammation.

In addition to liver benefits, elafibranor treatment also resulted in significant improvement in free choice diet induced HFpEF. Currently, there are no preclinical or clinical studies indicating that this dual PPARα/δ agonist has a direct effect on cardiac function. While clinical data are not available due to the limited development of PPARδ agonists, PPARα agonists, namely fibrates, are reported to either have no effect or decrease the risk of heart failure in parallel with their hypolipidemic effects [41]. Although preclinical studies suggest that activation of both PPARα and PPARδ alters cardiac expression of genes involved in cardiac metabolism and function [41], we did not detect any change with elafibranor, and cardiac fibrosis remained unchanged. This suggests that the improvement in heart failure would be related to other metabolic improvements by elafibranor. Although it was technically not possible to measure hamster-specific proteins (e.g. IL-1β, IL-18, TGF- β or natriuretic peptides), this would also exclude any contribution of cardiokines [42]. Crosstalk between the heart and adipose tissue, including fat mass and energy expenditure, may also play a role in obesity associated HFpEF [43]. However, we did not detect a significant body weight reduction in hamsters treated with elafibranor. Other studies in ob/ob or high fat fed NASH mouse model treated with elafibranor have shown significant reduction in body weight, but opposite effects on fat mass [44,45] and no effect on energy expenditure [45]. Nevertheless, the precise link between NASH and cardiac complications, and how NASH improvement benefits the heart, are poorly understood. Those mechanisms could be improvement of insulin resistance, visceral adiposity, low-grade inflammation, dyslipidemia, and oxidative stress [46]. Oxidative stress leads to endothelial dysfunction and atherosclerosis, which both contribute to cardiovascular complications. Although endothelial function could be studied on isolated aortic rings [33], the Golden Syrian hamster does not develop atherosclerotic lesions on high fat/cholesterol diet [47]. Therefore, a role of atherosclerosis in promoting HFpEF in the present model seems unlikely. Although we did not measure blood pressure in the present study, the Golden Syrian hamster strain is not spontaneously hypertensive [48] and free choice diet resulted in bridging fibrosis, but not cirrhosis. This would also exclude a contribution of hypertension [49] or portal hypertension [50] in promoting left ventricular dysfunction. Instead, the significant effects of both the free choice and elafibranor on hepatic gene expression and NAFLD activity score would suggest a prominent role of the liver. Liver is also recognized to be an endocrine organ that secretes hepatokines, such as fetuin-A and fibroblast growth factor 21, that potentially contributes to cardiovascular diseases [51]. Although it was beyond the scope of the present characterization of our free choice hamster model, further investigations will be required to discriminate the molecular mechanisms altering the heart-liver axis in the context of NASH and HFpEF.

## 5. Conclusion

Our data further demonstrate that the free choice diet-induced NASH hamster represents a robust alternative to the limitations of other rodent models for evaluating novel compounds targeting NASH and their potential benefits on cardiovascular disease. Further investigations are needed to discriminate the molecular mechanisms altering the liver-heart axis. Meanwhile, our preclinical model will be useful to demonstrate that an effective therapy targeting the liver can also improve HFpEF, as cardiovascular disease remains the leading cause of death in NASH patients.

Supplementary data to this article can be found online at https://doi.org/10.1016/j.metabol.2021.154707.

## Funding information

This study was funded by Physiogenex.

## CRediT authorship contribution statement

**François Briand:** Conceptualization, Methodology, Project administration, Supervision, Formal analysis, Validation, Visualization, Writing – original draft, Writing – review & editing. **Julie Maupoint:** Investigation, Formal analysis, Writing – review & editing. **Emmanuel Brousseau:** Investigation, Validation, Formal analysis. **Natalia Breyner:** Investigation, Formal analysis. **Mélanie Bouchet:** Investigation, Formal analysis. **Clément Costard:** Investigation, Formal analysis. **Thierry Leste-Lasserre:** Investigation, Validation, Formal analysis. **Mathieu Petitjean:** Investigation, Validation, Formal analysis. **Li Chen:** Investigation, Validation, Formal analysis. **Audrey Chabrat:** Investigation, Validation, Formal analysis. **Virgile Richard:** Investigation, Validation, Formal analysis. **Rémy Burcelin:** Conceptualization, Methodology, Writing – review & editing. **Caroline Dubroca:** Investigation, Formal analysis, Writing – review & editing. **Thierry Sulpice:** Conceptualization, Methodology, Writing – review & editing, Project administration.

## Declaration of competing interest

François Briand, Emmanuel Brousseau, Natalia Breyner, Mélanie Bouchet and Thierry Sulpice are employees of Physiogenex. Julie Maupoint, Caroline Dubroca, Clément Costard and Thierry Sulpice are employees of Cardiomedex. François Briand, Rémy Burcelin and Thierry

Sulpice have shares in Physiogenex. Thierry Sulpice and Rémy Burcelin have shares in Cardiomedex. Audrey Chabrat and Virgile Richard are employees of Sciempath Labo. Mathieu Petitjean and Li Chen are employees of PharmaNest.

## Acknowledgements

The authors thank colleagues and collaborators from Physiogenex (Dominique Lopes, and Paolo Demoor for animal care, Mylène Bernes, Marion Xolin and Loïc Pellissier for technical assistance, and Sura Setau for audits and quality control of experiments and data) and from Inserm 1048/Anexplo platform (Cyrielle Magne-Alibert, Deborah Campayo and Laurent Monbrun).

## References

[1] Johnson RJ, Stenvinkel P, Martin SL, Jani A, Sánchez-Lozada LG, Hill JO, et al. Redefining metabolic syndrome as a fat storage condition based on studies of comparative physiology. Obesity. 2013;21(4):659–64.
[2] Nolan CJ, Prentki M. Insulin resistance and insulin hypersecretion in the metabolic syndrome and type 2 diabetes: time for a conceptual framework shift. Diab Vasc Dis Res. 2019;16(2):118–27.
[3] Lev-Ran A. Human obesity: an evolutionary approach to understanding our bulging waistline. Diabetes Metab Res Rev. 2001;17(5):347–62.
[4] Apovian CM. Obesity: definition, comorbidities, causes, and burden. Am J Manag Care. 2016;22(7 Suppl):s176–85.
[5] Said S, Mukherjee D, Whayne TF. Interrelationships with metabolic syndrome, obesity and cardiovascular risk. Curr Vasc Pharmacol. 2016;14(5):415–25.
[6] Hardy T, Anstee QM, Day CP. Nonalcoholic fatty liver disease: new treatments. Curr Opin Gastroenterol. 2015;31(3):175–83.
[7] Anstee QM, Reeves HL, Kotsiliti E, Govaere O, Heikenwalder M. From NASH to HCC: current concepts and future challenges. Nat Rev Gastroenterol Hepatol. 2019;16(7):411–28.
[8] Tana C, Ballestri S, Ricci F, Di Vincenzo A, Ticinesi A, Gallina S, et al. Cardiovascular risk in non-alcoholic fatty liver disease: mechanisms and therapeutic implications. Int J Environ Res Public Health. 2019;16(17):3104.
[9] Anstee QM, Mantovani A, Tilg H, Targher G. Risk of cardiomyopathy and cardiac arrhythmias in patients with nonalcoholic fatty liver disease. Nat Rev Gastroenterol Hepatol. 2018;15(7):425–39.
[10] Packer M. Atrial fibrillation and heart failure with preserved ejection fraction in patients with nonalcoholic fatty liver disease. Am J Med. 2020;133(2):170–7.
[11] Lee H, Kim G, Choi YJ, Huh BW, Lee BW, Kang ES, et al. Association between non-alcoholic steatohepatitis and left ventricular diastolic dysfunction in type 2 diabetes mellitus. Diabetes Metab J. 2020;44(2):267–76.
[12] Yoshihisa A, Sato Y, Yokokawa T, Sato T, Suzuki S, Oikawa M, et al. Liver fibrosis score predicts mortality in heart failure patients with preserved ejection fraction. ESC Heart Fail. 2018;5(2):262–70.
[13] Pisto P, Santaniemi M, Bloigu R, Ukkola O, Kesäniemi YA. Fatty liver predicts the risk for cardiovascular events in middle-aged population: a population-based cohort study. BMJ Open. 2014;4(3):e004973.
[14] Angulo P, Kleiner DE, Dam-Larsen S, et al. Liver fibrosis, but no other histologic features, is associated with long-term outcomes of patients with nonalcoholic fatty liver disease. Gastroenterology. 2015;149(2):389–97.
[15] Imajo K, Yoneda M, Kessoku T, Ogawa Y, Maeda S, Sumida Y, et al. Rodent models of nonalcoholic fatty liver disease/nonalcoholic steatohepatitis. Int J Mol Sci. 2013;14(11):21833–57.
[16] Ibrahim SH, Hirsova P, Malhi H, Gores GJ. Animal models of nonalcoholic steatohepatitis: eat, delete, and inflame. Dig Dis Sci. 2016;61(5):1325–36.
[17] Denk H, Abuja PM, Zatloukal K. Animal models of NAFLD from the pathologist's point of view. Biochim Biophys Acta Mol Basis Dis. 2019;1865(5):929–42.
[18] Takahashi S, Fukami T, Masuo Y, Brocker CN, Xie C, Krausz KW, et al. Cyp2c70 is responsible for the species difference in bile acid metabolism between mice and humans. J Lipid Res. 2016;57(12):2130–7.
[19] Gottlieb A, Canbay A. Why bile acids are so important in non-alcoholic fatty liver disease (NAFLD) progression. Cells. 2019;8(11):1358.
[20] Briand F, Brousseau E, Quinsat M, Burcelin R, Sulpice T. Obeticholic acid raises LDL-cholesterol and reduces HDL-cholesterol in the Diet-Induced NASH (DIN) hamster model. Eur J Pharmacol. 2018;818:449–56.
[21] Briand F. The use of dyslipidemic hamsters to evaluate drug-induced alterations in reverse cholesterol transport. Curr Opin Investig Drugs. 2010;11(3):289–97.
[22] Galeazzi R, Javitt NB. Bile acid excretion: the alternate pathway in the hamster. J Clin Invest. 1977;60(3):693–701.
[23] Cipriani S, Mencarelli A, Palladino G, Fiorucci S. FXR activation reverses insulin resistance and lipid abnormalities and protects against liver steatosis in Zucker (fa/fa) obese rats. J Lipid Res. 2010;51(4):771–84.
[24] Xu Y, Li F, Zalzala M, et al. Farnesoid X receptor activation increases reverse cholesterol transport by modulating bile acid composition and cholesterol absorption in mice. Hepatology. 2016;64(4):1072–85.
[25] Siddiqui MS, Van Natta ML, Connelly MA, et al. Impact of obeticholic acid on the lipoprotein profile in patients with non-alcoholic steatohepatitis. J Hepatol. 2020;72(1):25–33.
[26] Westerouen Van Meeteren MJ, Drenth JPH, Tjwa ETTL. Elafibranor: a potential drug for the treatment of nonalcoholic steatohepatitis (NASH). Expert Opin Investig Drugs. 2020;29(2):117–23.
[27] Briand F, Brousseau E, Maupoint J, Dubroca C, Costard C, Breyner N, et al. Liraglutide shows superior cardiometabolic benefits than lorcaserin in a novel free choice diet-induced obese rat model. Eur J Pharmacol. 2020;882:173316.
[28] Briand F, Thiéblemont Q, Muzotte E, Sulpice T. High-fat and fructose intake induces insulin resistance, dyslipidemia, and liver steatosis and alters in vivo macrophage-to-feces reverse cholesterol transport in hamsters. J Nutr. 2012;142(4):704–9.
[29] Kleiner DE, Brunt EM, Van Natta M, Behling C, Contos MJ, Cummings OW, et al. Design and validation of a histological scoring system for nonalcoholic fatty liver disease. Hepatology. 2005;41(6):1313–21.
[30] Chomczynski P, Sacchi N. Single-step method of RNA isolation by acid guanidinium thiocyanate-phenol-chloroform extraction. Anal Biochem. 1987 Apr;162(1):156–9.
[31] Bustin SA, Benes V, Garson JA, Hellemans J, Huggett J, Kubista M, et al. The MIQE guidelines: minimum information for publication of quantitative real-time PCR experiments. Clin Chem. 2009 Apr;55(4):611–22.
[32] Livak KJ, Schmittgen TD. Analysis of relative gene expression data using real-time quantitative PCR and the 2(-delta delta C(T)) method. Methods. 2001 Dec;25(4):402–8.
[33] Watanabe S, Kumazaki S, Kusunoki K, Inoue T, Maeda Y, Usui S, et al. A high-fat and high-cholesterol diet induces cardiac fibrosis, vascular endothelial, and left ventricular diastolic dysfunction in SHRSP5/Dmcr rats. J Atheroscler Thromb. 2018;25(5):439–53.
[34] Thakare R, Alamoudi JA, Gautam N, Rodrigues AD, Alnouti Y. Species differences in bile acids I. Plasma and urine bile acid composition. J Appl Toxicol. 2018;38(10):1323–35.
[35] Di Lascio N, Kusmic C, Stea F, Lenzarini F, Barsanti C, Leloup A, et al. Longitudinal micro-ultrasound assessment of the ob/ob mouse model: evaluation of cardiovascular, renal and hepatic parameters. Int J Obes (Lond). 2018;42(3):518–24.
[36] Miyaoka Y, Jin D, Tashiro K, Masubuchi S, Ozeki M, Hirokawa F, et al. A novel hamster nonalcoholic steatohepatitis model induced by a high-fat and high-cholesterol diet. Exp Anim. 2018;67(2):239–47.
[37] Lackner C, Gogg-Kamerer M, Zatloukal K, Stumptner C, Brunt EM, Denk H. Ballooned hepatocytes in steatohepatitis: the value of keratin immunohistochemistry for diagnosis. J Hepatol. 2008;48(5):821–8.
[38] Gao L, Zhang Z, Zhang P, Yu M, Yang T. Role of canonical Hedgehog signaling pathway in liver. Int J Biol Sci. 2018;14(12):1636–44.
[39] Ratziu V, Harrison SA, Francque S, Bedossa P, Lehert P, Serfaty L, et al. Elafibranor, an agonist of the peroxisome proliferator-activated receptor-α and -δ, induces resolution of nonalcoholic steatohepatitis without fibrosis worsening. Gastroenterology. 2016;150(5):1147–59.
[40] Staels B, Rubenstrunk A, Noel B, Rigou G, Delataille P, Millatt LJ, et al. Hepatoprotective effects of the dual peroxisome proliferator-activated receptor alpha/delta agonist, GFT505, in rodent models of nonalcoholic fatty liver disease/nonalcoholic steatohepatitis. Hepatology. 2013;58(6):1941–52.
[41] Pol CJ, Lieu M, Drosatos K. PPARs: protectors or opponents of myocardial function? PPAR Res. 2015;2015:835985.
[42] Wu YS, Zhu B, Luo AL, Yang L, Yang C. The role of cardiokines in heart diseases: beneficial or detrimental? Biomed Res Int. 2018;2018:8207058.
[43] Oh A, Okazaki R, Sam F, Valero-Muñoz M. Heart failure with preserved ejection fraction and adipose tissue: a story of two tales. Front Cardiovasc Med. 2019;2(6):110.
[44] Roth JD, Veidal SS, Fensholdt LKD, Rigbolt KTG, Papazyan R, Nielsen JC, et al. Combined obeticholic acid and elafibranor treatment promotes additive liver histological improvements in a diet-induced ob/ob mouse model of biopsy-confirmed NASH. Sci Rep. 2019;9(1):9046.
[45] Tsai HC, Chang FP, Li TH, Liu CW, Huang CC, Huang SF, et al. Elafibranor inhibits chronic kidney disease progression in NASH mice. Biomed Res Int. 2019;2019:6740616.
[46] El Hadi H, Di Vincenzo A, Vettor R, Rossato M. Relationship between heart disease and liver disease: a two-way street. Cells. 2020;9(3):567.
[47] Dillard A, Matthan NR, Lichtenstein AH. Use of hamster as a model to study diet-induced atherosclerosis. Nutr Metab (Lond). 2010;7:89.
[48] Thomas CL, Artwohl JE, Suzuki H, et al. Initial characterization of hamsters with spontaneous hypertension. Hypertension. 1997;30(2 Pt 1):301–4.
[49] Sorrentino MJ. The evolution from hypertension to heart failure. Heart Fail Clin. 2019;15(4):447–53.
[50] Stundiene I, Sarnelyte J, Norkute A, Aidietiene S, Liakina V, Masalaite L, et al. Liver cirrhosis and left ventricle diastolic dysfunction: systematic review. World J Gastroenterol. 2019;25(32):4779–95.
[51] Jung TW, Yoo HJ, Choi KM. Implication of hepatokines in metabolic disorders and cardiovascular diseases. BBA Clin. 2016;5:108–13.